Fault Modeling and Analysis of Grid-connected Inverters with Decoupled Sequence Control

Zhang, Qi; Liu, Dong; Liu, Zhou; Chen, Zhe

Published in:
IEEE Transactions on Industrial Electronics

DOI (link to publication from Publisher):
10.1109/TIE.2021.3088378

Publication date:
2022

Document Version
Accepted author manuscript, peer reviewed version

Fault Modeling and Analysis of Grid-connected Inverters with Decoupled Sequence Control

Qi Zhang, *Student Member, IEEE*, Dong Liu, *Senior Member, IEEE*, Zhou Liu, *Senior Member, IEEE*, and Zhe Chen, *Fellow, IEEE*

***Abstract*—With an increasing number of inverter-interfaced generators (IIGs), the power system is undergoing massive shifts towards the power electronic dominated power system. Such paradigm change poses significant challenges to existing fault analysis theory and the protection system, as a result of the disparate short-circuit response. Given this, the fault analysis theory needs to be further investigated and expanded to address issues arising from the new grid paradigm. Under this context, this paper proposes an analytic model for short-circuit analysis of IIGs with decoupled sequence control (DSC) based on the Laplace transform. With the proposed model, the analytic fault current expression can be obtained and the fault characteristic can be analyzed. Compared with existing studies, the proposed model distinguishes itself by three key merits. First, the proposed model takes into account the delay feature of the controller, which enables transient analysis. Second, the model covers the impact of controller parameters and low voltage ride through (LVRT) strategy in detail which is missing in the most existing literature. Third, the proposed model provides a theoretical foundation of IIGs with DSC in the fault analysis, which makes it more applicable for the protection setup issues in reality. In the end, the correctness and feasibility of the proposed model is validated by the simulation and experimental result.**

***Index Terms*—Fault analysis, inverter-interfaced generators, renewable energy sources, decoupled sequence control (DSC).**

I. Introduction

The modern power system is moving towards the power electronic dominated power system due to the significant change in generation forms [1]. This development trend poses challenges for the existing fault analysis theory and the protection system because of the significantly different fault response between synchronous generators (SGs) and IIGs. For instance, the steady-state fault current of SGs are normally larger than 10 p.u. but they are limited to only 1-2 p.u. of IIGs to protect the expensive semiconductor switching devices [2]–[4]. Those challenges are critical in fault analysis of the power electronic dominated power system because almost all the fault currents are contributed by IIGs. Normally, fault characteristics of IIGs cannot be overlooked when IIGs supply about 10% or more of the feeder load [5]. Therefore, the conventional fault analysis theory needs to be further expanded to adapt to the new grid form.

As the cornerstone of fault analysis theory, the fault modeling study aims to present simple and effective models for generators to calculate a series of critical parameters used in power system planning, designing, and protection system setup, such as the maximum inrush currents, RMS of steady-state fault current, etc. [6]. Traditional synchronous generators have strong inertia and the ability to withstand high inrush currents, so they are usually modeled as constant voltage sources in the fault analysis. However, the traditional modeling method for SGs is not applicable for the fault analysis of IIGs since the fault response characteristic of IIGs are more complicated than that of SGs as follows.

(1) The fault current of IIGs changes faster than that of SGs because of fast-response controllers of IIGs and their characteristics are strongly related to the parameters of the employed controller [7], [8].
(2) The fault behavior of IIGs is more complicated than SGs due to the requirements of Grid Codes (GC) [7]–[9].
(3) The interaction of IIGs with the grid conditions obviously affects the fault response of IIGs [10].

The study on fault modeling for IIGs has gained much attention in recent years. An early study on fault modeling of IIGs was published in 2005 [5]. It shows that the fault current of IIGs varies considerably due to the fast response feature of the employed controller. The fault period is divided into three phases in this study, i.e., the sub-transient phase (first cycle), the transient phase (3-10 cycles), and the steady-state phase. The definition of the fault period in [5] is well inherited in the subsequent studies [9], [11]–[15]. Moreover, based on the state-space model of inverter and grid, reference [5] proposes an iterative algorithm to estimate the RMS value of fault currents, in which the current limitation and the interaction of IIGs with grid are both taken into consideration. However, the transient phase of fault responses is ignored so that the inrush current cannot be calculated by using the proposed method. In addition, the Low Voltage Ride Through (LVRT) control strategy are disregarded.

Extensive research has been conducted on fault modeling of IIGs [7], [15]–[18], from 2007 to 2014 primarily by a research group in Imperial College. To investigate the fault behavior of an inverter-only supplied micro-grid by computer simulation and numerical analysis, IIGs are modeled as controlled current source with a parallel impedance to reconstruct fault currents [7]. Additionally, based on the controlled source concept, IIGs are modeled as PQ sources to estimate fault currents based on the steady-state power flow calculation [15], [16], [18]. However, these methods mentioned above do not take the LVRT control strategy into consideration. Moreover, they fail

to handle the transient phase analysis, so they can not be used to calculate the inrush current of IIGs.

A more comprehensive and representative research was published in 2018 [9], in which the fault models of IIGs with various control schemes including the constant current control (CCC), the decoupled current control (DCC), and the voltage-frequency droop control (V/FDC) are proposed. In reference [9], it points out the current limitation affects the fault current obviously, and the time constant of fault responses are strongly related to the control scheme. Besides, this study assumes that the controller of IIGs works perfectly in real time, thus the time of transient phase of IIGs is so small that it can be ignored. However, this assumption ignores the fact that sensors and filters inevitably introduce time delay to the control system, which makes it hardly applicable to practical applications.

Since existing literature mainly focuses on the steady phase of the fault response and ignores the transient phase of the fault response, the transient phase of IIGs' fault responses is still a missing point. In practical, IIGs can not respond to the grid condition changes in real-time due to the indispensable time delays of sensors, communications, filters, and controllers, which has been noticed and pointed out in [19]. Besides, the exact relationship between controller parameters and the fault response is not discussed in detail yet.

Moreover, most of the existing research focuses on the fault modeling of IIGs with DCC, but the fault modeling of IIGs with DSC is not discussed yet. Compared with DCC strategy, DSC strategy overcomes the problem of active-power oscillation [12] which may bring risks to the power system reliability. Given this, more and more IIGs with DSC are connected to the grid [20], especially with the increasing penetration of renewable integration. The fault modeling of IIGs with DSC is more challenging because 1) the control system is more complicated; 2) the time delay of the filters and the grid voltage estimating elements are too large to be ignored anymore. Accordingly, the fault modeling of IIGs with DCC cannot be used to analyze the fault characteristic of IIGs with DSC.

In order to address aforementioned issues, this paper proposes an analytic model for IIGs with DSC to investigate the fault current characteristic. The proposed model can be used to handle the transient analysis of fault responses because the delay feature of the control system is taken into consideration. In addition, the influence of controller parameters on fault current characteristics can be analyzed explicitly by using the proposed model. Moreover, the LVRT strategy are taken into consideration in the proposed model, which means the proposed model would be more applicable for the fault analysis of practical applications.

II. Decoupled Sequence Control of IIGs

The IIGs with DSC are shown in Fig. 1. The types of power filter in practical applications are usually different, for example, L, LC, or LCL, and the impacts from the type of filters on the fault current can be ignored because only the fundamental component of fault currents is normally

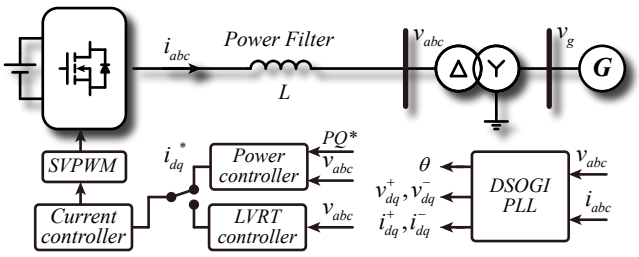

Fig. 1. The system configuration of IIGs and the block diagram of DSC.

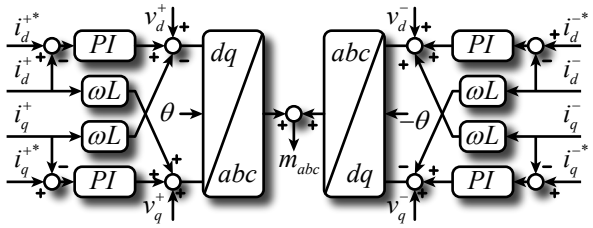

Fig. 2. Block diagram of the current controller.

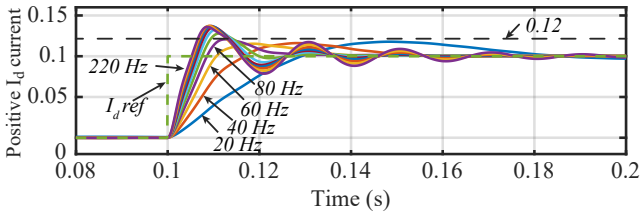

Fig. 3. The step response of the current controller with different cutoff frequency ω_c.

considered in fault analysis, so to guarantee the applicability of the proposed model, the L filter is used as an example to describe the proposed model. The transformer in this study is ideal to simplify the analysis. As illustrated in Fig. 1, the DSC generally consists of four parts: the current controller, the power controller, the LVRT controller, and the Double Second Order Generalized Integrator Phase Locked Loop (DSOGI-PLL) [20].

The current controller is composed of two decoupled current controllers (DCC) to independently control the sequence components of currents as shown in Fig. 2. The parameter of the current controller is critical in the fault analysis of IIGs, and there are many tuning methods for obtaining parameters of the current controller. Thus, it is very hard to build a unified model to represent all kinds of parameters. To guarantee the universality of the proposed model, the most prevalent tuning method [21], which is suggested by the IEEE technological report [1] and the published modeling guidelines [22], is used to tune the PI controller in the proposed model. Based on the conclusion in [22], the parameter of PI controllers can be obtained based on (1).

$$\begin{cases} k_p = \omega_c L \\ k_i = \omega_c R \end{cases} \tag{1}$$

In (1), the cutoff frequency ω_c is the only parameter to be determined. The rising time of the controller reduces with the increase of ω_c, but the overshoot increases in the meantime,

as shown in Fig. 3. Besides, when the ω_c is greater than 80 Hz, the influence of ω_c on the dynamic performance would be minor. In view of above points, it is better to select ω_c in the range under 80 Hz.

In normal conditions, the power controller generates the reference input based on the set point of active and reactive power labeled as PQ^* in Fig. 1. The negative current reference input which are labeled as i_d^{-*}, i_q^{-*} in Fig. 2 are set to zero and the positive current reference input labeled as i_d^{+*}, i_q^{+*} are calculated based on the instantaneous power theory [23] shown as (2).

$$\begin{cases} P = v_q^+ i_q^+ + v_d^+ i_d^+ \\ Q = v_d^+ i_q^+ - v_q^+ i_d^+ \end{cases} \tag{2}$$

In fault conditions, the power controller is disabled and the reference input of current controllers are generated by the LVRT controller as shown in Fig. 1, based on the instantaneous active and reactive power under unbalanced grid conditions [24]:

$$\begin{cases} P = P_0 + P_{c2}\cos(2\omega t) + P_{s2}\sin(2\omega t) \\ Q = Q_0 + Q_{c2}\cos(2\omega t) + Q_{s2}\sin(2\omega t) \end{cases} \tag{3}$$

where P_0, Q_0 are the average values of active and reactive power and $P_{c2}, Q_{c2}, P_{s2}, Q_{s2}$ are amplitudes of the individual second harmonic components of power. They can be expressed as (4) in the synchronous rotating DQ frame.

$$\begin{bmatrix} P_0 \\ P_{c2} \\ P_{s2} \\ Q_0 \\ Q_{c2} \\ Q_{s2} \end{bmatrix} = \frac{3}{2} \begin{bmatrix} v_d^+ & v_q^+ & v_d^- & v_q^- \\ v_d^- & v_q^- & v_d^+ & v_q^+ \\ v_q^- & -v_d^- & -v_q^+ & v_d^+ \\ v_q^+ & -v_d^+ & v_q^- & -v_d^- \\ v_q^- & -v_d^- & v_q^+ & -v_d^+ \\ -v_d^- & -v_q^- & v_d^+ & v_q^+ \end{bmatrix} \begin{bmatrix} i_d^+ \\ i_q^+ \\ i_d^- \\ i_q^- \end{bmatrix} \tag{4}$$

The coefficient matrix in (4) is irreversible so the reference input of current controllers cannot be calculated directly with the given $P_0, P_{c2}, P_{s2}, Q_0, Q_{c2}, Q_{s2}$. The flexible power control strategy expressed as (5) was proposed in [25] to overcome this problem.

$$\begin{bmatrix} i_d^{+*} \\ i_q^{+*} \\ i_d^{-*} \\ i_q^{-*} \end{bmatrix} = \frac{2}{3} \begin{bmatrix} e_d^+ & e_q^+ \\ e_q^+ & -e_d^+ \\ -Ke_d^- & Ke_q^- \\ -Ke_q^- & -Ke_d^- \end{bmatrix} \begin{bmatrix} \frac{P_0^*}{D} \\ \frac{Q_0^*}{E} \end{bmatrix} \tag{5}$$

where:

$$\begin{cases} K = 0, \pm 1 \\ D = \left(e_d^+\right)^2 + \left(e_q^+\right)^2 - K\left[\left(e_d^-\right)^2 + \left(e_q^-\right)^2\right] \\ E = \left(e_d^+\right)^2 + \left(e_q^+\right)^2 + K\left[\left(e_d^-\right)^2 + \left(e_q^-\right)^2\right] \end{cases}$$

The factor K is used for denoting the control strategy during grid faults. If K is set to zero, only positive current will be injected to the grid. The oscillation of active power will be eliminated when K equals to 1, and for K equals to -1, the output reactive power of inverters keeps constant. To enhance the reliability of the power system, grid codes stipulate the behavior of IIGs under faults, for example, the Danish grid

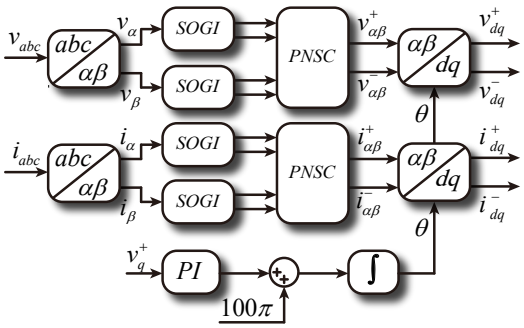

Fig. 4. Block diagram of the DSOGI-PLL with positive and negative sequence components calculation model (PNSC).

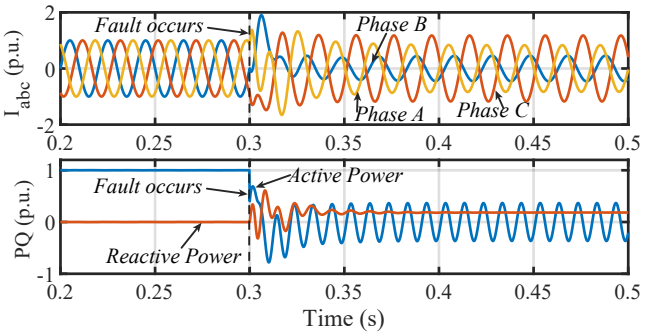

Fig. 5. The characteristic of the LVRT control strategy.

code [26] defines that IIGs should firstly inject reactive power to grid and the amount of injected reactive power is related to the voltage of connected bus. In addition, as discussed in [1], [27], [28], lack of negative sequence fault current contribution from the IIGs may cause mis-operation of protection system during certain unbalanced fault conditions [12]. If the K equals to -1, the IIGs can inject negative currents to the gird, so the mis-operation of protection system can be avoided. With these two considerations above, the control factor K is set to -1 under faults in this study and the characteristic of the LVRT controller is shown in Fig. 5.

The calculated reference current may be very large which is beyond the ability of IIGs, thus IIGs require the current limiter to avoid over current. The limiter is designed as:

$$\begin{cases} i_{dq}^{+*} = \begin{cases} i_{dq_L}^{+*}, M \le 1.2 \\ 1.2\dfrac{i_{dq_L}^{+*}}{M}, M > 1.2 \end{cases} \\ i_{dq}^{-*} = \begin{cases} i_{dq_L}^{-*}, M \le 1.2 \\ 1.2\dfrac{i_{dq_L}^{-*}}{M}, M > 1.2 \end{cases} \\ M = \sqrt{(i_{d_L}^+)^2 + (i_{q_L}^+)^2} + \sqrt{(i_{d_L}^-)^2 + (i_{q_L}^-)^2} \end{cases} \tag{6}$$

where i_{dq}^{+*}, i_{dq}^{-*} are reference values for the current controller; and $i_{dq_L}^{+*}, i_{dq_L}^{-*}$ are results calculated by the LVRT controller.

Due to the high performance under unbalanced grid conditions, the DSOGI-PLL shown in Fig. 4 is used in DSC to estimate the phase angle, sequence components of the grid

voltage, and the sequence components of the injected current of IIGs. More details about DSOGI-PLL can be found in [29].

III. Fault Modeling of IIGs with DSC

Define the DQ transfer matrix as $T_{dq}(\theta)$, the column vector in double DQ frame as $\boldsymbol{x_{dq}}$ where $\boldsymbol{x}$ can be voltage v or current i, and the sign matrix as $\boldsymbol{J}$:

$$T_{dq}(\theta) = \begin{bmatrix} \cos(\theta) & \sin(\theta) \\ -\sin(\theta) & \cos(\theta) \end{bmatrix} \tag{7}$$

$$\boldsymbol{x_{dq}} = \left[x_d^+, x_q^+, x_d^-, x_q^-\right]^T \tag{8}$$

$$\boldsymbol{J} = \begin{bmatrix} 0 & -1 & 0 & 0 \\ 1 & 0 & 0 & 0 \\ 0 & 0 & 0 & 1 \\ 0 & 0 & -1 & 0 \end{bmatrix} \tag{9}$$

A. The transfer function model of DSOGI-PLL

Since the SOGI in DSOGI-PLL introduces a considerable delay to the voltage and current estimating, it is necessary to construct a correct model to illustrate the delay feature. In the following contents, the transfer function of DSOGI-PLL will be analyzed to obtain the relationship between the estimated and true values.

Define the column vector $\hat{\boldsymbol{x}}_{\boldsymbol{\alpha\beta}}$ to denote the estimated sequence components of variable $\boldsymbol{x}$, which can be voltage $\boldsymbol{v}$ or current $\boldsymbol{i}$ in $\alpha\beta$ domain and the column vector $\boldsymbol{x_{\alpha\beta}}$ to denote the true value of variable in $\boldsymbol{x}$, which is obtained by using Clarke transformation from three-phase voltages or three-phase currents.

$$\hat{\boldsymbol{x}}_{\boldsymbol{\alpha\beta}} = \left[x_\alpha^+, x_\beta^+, x_\alpha^-, x_\beta^-\right]^T \tag{10}$$

$$\boldsymbol{x_{\alpha\beta}} = \left[x_\alpha, x_\beta\right]^T \tag{11}$$

where the superscripts $+, -$ are used to denote the positive and negative sequence components, respectively.

The transfer function of the DSOGI in static two-phase $\alpha\beta$ frame is given in (12) [20], [29].

$$\hat{\boldsymbol{X}}_{\boldsymbol{\alpha\beta}}(s) = \boldsymbol{K}\boldsymbol{X}_{\boldsymbol{\alpha\beta}}(s) \tag{12}$$

$$\boldsymbol{K} = \frac{1}{2}\begin{bmatrix} D(s) & -Q(s) \\ Q(s) & D(s) \\ D(s) & Q(s) \\ -Q(s) & D(s) \end{bmatrix}$$

where, $D(s), Q(s)$ are the transfer function of SOGI, as shown in (13):

$$\begin{cases} D(s) = \dfrac{k\omega s}{s^2 + k\omega s + \omega^2} \\ Q(s) = \dfrac{k\omega^2}{s^2 + k\omega s + \omega^2} \end{cases} \tag{13}$$

Apply the Park transformation to (12), (14) can be obtained.

$$\hat{\boldsymbol{x}}_{\boldsymbol{dq}} = \overbrace{\left[\begin{array}{c|c} T_{dq}(\theta) & \mathbf{0} \\ \hline \mathbf{0} & T_{dq}(-\theta) \end{array}\right]}^{\boldsymbol{M}} \left(\mathcal{L}\{\boldsymbol{K}\}^{-1} * \boldsymbol{x_{\alpha\beta}}\right) \tag{14}$$

where the operator '$*$' means the convolution of two functions.

Because the $\boldsymbol{x_{\alpha\beta}}$ is the representation of three-phase variables in the $\alpha\beta$ domain, and the $\boldsymbol{x_{dq}}$ is the representation of three-phase variables in the double DQ frame, the relationship between $\boldsymbol{x_{\alpha\beta}}$ and $\boldsymbol{x_{dq}}$ can be expressed as (15) by using the inverse Park and Clarke transformation.

$$\boldsymbol{x_{\alpha\beta}} = \overbrace{\begin{bmatrix} 1 & 0 & 1 & 0 \\ 0 & 1 & 0 & 1 \end{bmatrix}}^{\boldsymbol{A}} \overbrace{\left[\begin{array}{c|c} T_{dq}^{-1}(\theta) & \mathbf{0} \\ \hline \mathbf{0} & T_{dq}^{-1}(-\theta) \end{array}\right]}^{\boldsymbol{M^{-1}}} \boldsymbol{x_{dq}} \tag{15}$$

Combine (7), (14), and (15), it can be obtained that:

$$\hat{\boldsymbol{x}}_{\boldsymbol{dq}} = \boldsymbol{M}(\boldsymbol{\mathcal{L}\{K\}^{-1}} * \boldsymbol{AM^{-1}x_{dq}}) \tag{16}$$

Based on the modulation theory [30], if $\mathcal{L}\{f(t)\} = F(s)$,

$$\mathcal{L}\{f(t)\cos(\omega t)\} = \frac{1}{2}\left(F(s - j\omega) + F(s + j\omega)\right) \tag{17}$$

$$\mathcal{L}\{f(t)\sin(\omega t)\} = \frac{1}{2j}\left(F(s - j\omega) - F(s + j\omega)\right) \tag{18}$$

Apply the Laplace transformation to (16) with (17) and (18), the transfer function of the DSOGI-PLL $\boldsymbol{H}(s)$ can be obtained as (19):

$$\boldsymbol{H}(s) = H_f \begin{bmatrix} B_{11} & \cdots & B_{14} \\ \vdots & \ddots & \vdots \\ B_{41} & \cdots & B_{44} \end{bmatrix} \tag{19}$$

where:

$$\begin{aligned} H_f &= \frac{k\omega}{2s^4 + 4k\omega s^3 + 2(k^2+4)\omega^2 s^2 + 8k\omega^3 s + 2k^2\omega^4} \\ B_{11} &= s^3 + k\omega s^2 + 4\omega^2 s + 2k\omega^3 \\ B_{12} &= -k\omega^2 s \\ B_{13} &= (s + k\omega)s^2 \\ B_{14} &= (2s + k\omega)\omega s \\ B_{22} &= B_{33} = B_{44} = B_{11} \\ B_{21} &= B_{34} = -B_{43} = -B_{12} \\ B_{31} &= B_{42} = B_{24} = B_{13} \\ B_{41} &= -B_{23} = -B_{32} = B_{14} \end{aligned}$$

and the k and ω are constant parameters of the DSOGI.

B. Model of IIGs with the current controller

The mathematic model of IIGs in the time domain can be expressed as follows:

$$L\frac{di_{abc}}{dt} + Ri_{abc} = u_{abc} - v_{abc} \tag{20}$$

where i_{abc} is the inductor current; u_{abc} is the voltage generated by the converter; v_{abc} is the grid voltage.

By using Park and Laplace transformation, (20) can be transformed into (21):

$$\boldsymbol{U_{dq}(s)} = \left((sL + R)\boldsymbol{I} + \omega L\boldsymbol{J}\right)\boldsymbol{I_{dq}(s)} + \boldsymbol{V_{dq}(s)} \tag{21}$$

where $\boldsymbol{U_{dq}}, \boldsymbol{I_{dq}}, \boldsymbol{V_{dq}}$ are the output of current controller, inductor currents and gird voltages in the synchronous rotating DQ frame; $\boldsymbol{I}$ is the identity matrix.

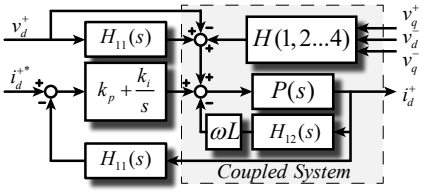

Fig. 6. The control block diagram of i_d^+

Based on the structure of current controller shown in Fig. 2, the mathematical model of current controller can be expressed as (22):

$$\boldsymbol{U_{dq}(s)} = \hat{\boldsymbol{V}}_{\boldsymbol{dq}}(\boldsymbol{s}) + \omega L \boldsymbol{J} \hat{\boldsymbol{I}}_{\boldsymbol{dq}}(\boldsymbol{s}) + (\boldsymbol{I}^*_{\boldsymbol{dq}}(\boldsymbol{s}) - \hat{\boldsymbol{I}}_{\boldsymbol{dq}}(\boldsymbol{s}))PI(s) \tag{22}$$

where $\hat{\boldsymbol{V}}, \hat{\boldsymbol{I}}$ are the estimated grid voltages and inductor currents. $PI(s)$ is the transfer function of the PI controller.

Combine (19), (21) and (22), the transfer function model of IIGs with DSC can be obtained as (23).

$$\begin{aligned}(Ls+R)\boldsymbol{II_{dq}(s)} = &(\boldsymbol{i^*_{dq}(s)} - \boldsymbol{HI_{dq}(s)})PI(s) \\ &+ (\boldsymbol{H}-\boldsymbol{I})\boldsymbol{V_{dq}(s)} \\ &+ \omega L \boldsymbol{J}(\boldsymbol{H}-\boldsymbol{I})\boldsymbol{I_{dq}(s)}\end{aligned} \tag{23}$$

Obviously, the part $Ls + R$ is the transfer function of the power filter. To obtain a more general model of IIGs with DSC, it is useful to replace this part with a general form as expressed as (24). Then, the model (23) can be rewritten as (25).

$$P(s) = \frac{1}{R}\frac{1}{\tau s+1}, \tau = \frac{L}{R} \tag{24}$$

$$\begin{aligned}\frac{1}{P(s)}\boldsymbol{II_{dq}(s)} = &(\boldsymbol{i^*_{dq}(s)} - \boldsymbol{HI_{dq}(s)})PI(s) \\ &+ (\boldsymbol{H}-\boldsymbol{I})\boldsymbol{V_{dq}(s)} \\ &+ \omega L \boldsymbol{J}(\boldsymbol{H}-\boldsymbol{I})\boldsymbol{I_{dq}(s)}\end{aligned} \tag{25}$$

C. Fault Analysis model of IIGs with DSC

Based on the analysis in the above section, the mathematic model of IIGs with DSC has been obtained as shown in Fig. (6). However, it is too complicated to apply the inverse Laplace transform for the analysis of fault current characteristics. Accordingly, it is necessary to simplify this model for obtaining the time domain function of fault currents. Here, the model is simplified from two aspects including 1) the transfer function $\boldsymbol{H}_{11}(s)$ of DSOGI-PLL in (19) and 2) the coupled system shown in Fig. (6).

By using the balancing-free square-root algorithm proposed in [31], the transfer function $\boldsymbol{H}_{11}(s)$ can be simplified to (26).

$$H(s) = \frac{K}{s+K}, K = 233.5; \tag{26}$$

Based on the final value theorem, in the transfer function matrix $\boldsymbol{H}$, only the final value of the diagonal element equals to one, which means that those none-diagonal transfer functions only introduces transient to system and has no effect on the steady-state output. In addition, if only the steady-state features are considered, the transfer function of the whole coupled system is $P(s)$. Thus, the coupled system can be simplified to $P_m(s)$ as (27), which only has a larger time constant compared with the system $P(s)$.

$$P_m(s) = \frac{1}{R}\frac{1}{2\tau s+1} \tag{27}$$

Replace $H_{11}(s)$ and $P(s)$ with $H(s)$ and $P_m(s)$, the mathematical model of IIGs shown in (25) can be simplified to a typical second order system as (28).

$$\begin{cases} C_1(s) = \dfrac{i_d^+}{i_d^{+*}} = \dfrac{\omega_c(s+K)}{s^2+Ks+K\omega_c} \\ C_2(s) = \dfrac{i_d^+}{v_d^+} = \dfrac{s^2}{(Ls+R)(s^2+Ks+K\omega_c)} \end{cases} \tag{28}$$

By using the inverse Laplace transform, the step response of the IIGs with DSC can be expressed as (29):

$$\begin{cases} f_1(t) = \mathcal{L}^{-1}\{C_1(s)\} \\ \qquad = 1 + Ne^{-\epsilon\omega_n t}\sin(A\omega_n t - \phi_1) \\ f_2(t) = \mathcal{L}^{-1}\{C_2(s)\} \\ \qquad = -RA^2M^2e^{-t/\tau} + Me^{-\epsilon\omega_n t}\sin(A\omega_n t + \phi_2) \end{cases} \tag{29}$$

where:

$$\begin{cases} \omega_n = \sqrt{2K\pi\omega_c}, \epsilon = \sqrt{\dfrac{K}{8\pi\omega_c}}, N = \dfrac{1}{2\epsilon A} \\ \phi_1 = \arctan(\dfrac{2\epsilon A}{\mid 2\epsilon^2 - 1 \mid}), \phi_2 = \arctan(\dfrac{A}{\omega_n\tau - \epsilon}) \\ A = \sqrt{1-\epsilon^2}, M = \dfrac{1}{AR\sqrt{(\omega_n\tau-\epsilon)^2 + A^2}} \end{cases} \tag{30}$$

D. Comparison of the proposed model with the existing methods

As mentioned in the introduction, various fault modeling methods have been published in previous studies. A comparison of the proposed model with other existing models is summarized in Table. I. It can be seen from Table. I, the proposed model distinguishes itself from three key merits. First, the proposed model takes into account the delay feature of the controller, which enables transient analysis. Second, the model covers the impact of controller parameters and low voltage ride through (LVRT) strategy in detail which is not discussed in the most existing literature. Third, the proposed model establishes a theoretical foundation of IIGs with DSC in the fault analysis, which makes it more applicable for protection setup issues in reality.

IV. Simulation and Experimental Verification

A. Simulation Verification

In order to verify the proposed model, a 250 kVA IIG is established in Simulink/MATLAB. The test system is shown in Fig. 7. Parameters of simulation model are listed in Table. II.

TABLE I
THE COMPARISON OF THE PROPOSED MODEL WITH THE EXISTING MODEL.

Model in	Types	Transient analysis	Current limitation	Consider LVRT	Controller	Consider delay
[5]	Iterative algorithm	Not support	Yes	Not	DCC	Not
[7]	Iterative algorithm	Not support	Yes	Not	DCC	Not
[9]	Analytic model	Support	Yes	Not	DCC	Not
[11]	Equivalent circuit model	Not support	Yes	Not	DCC	Not
[12]	Iterative algorithm	Support	Yes	Yes	DCC, DSC	Not
[15]–[18]	Equivalent circuit model	Not support	Yes	Not	DCC	Not
Proposed	Analytical model	Support	Yes	Yes	DSC	Yes

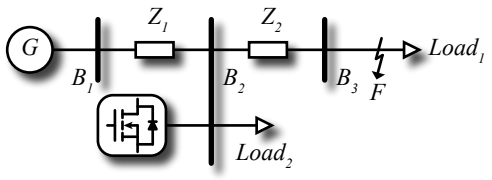

Fig. 7. The topology diagram of the test system in simulation

TABLE II
PARAMETERS OF SIMULATION MODEL

Parameters	Values
Grid voltage	10 kV
Z_1 (positive sequence)	1.5294 + j19.8753 Ω
Z_1 (negative sequence)	19.32 + j64.8173 Ω
Z_2 (positive sequence)	0.1273 + j2.9333 Ω
Z_2 (negative sequence)	3.864 + j12.9635 Ω
$Load_1$	0.5 MW
$Load_2$	10 kW
Inverter side AC voltage	0.38 kV
Rated Power	0.25 MVA
Voltage of DC source	0.75 kV
System frequency	50 Hz
Total resistance of LCL filter	38 mΩ
Total inductance of LCL filter	0.25 mH
Capacitance of LCL filter	200 uF
Cutoff frequency of current controller	80 Hz

1) Fault response comparison between DCC and DSC: Fig. 8 presents the simulation results of the fault response of the IIGs with DCC and DSC under three-phase asymmetrical fault. In Fig. 8, the IIGs with both DCC and DSC work under normal conditions and inject active power to the grid before 0.3s; the two phases (BC) to ground fault occurs at 0.3s and changes the grid voltage to unbalance. Comparing Fig. 8(b) and Fig. 8(c), the following can be obtained. 1) With DCC, the response speed is so fast that the transient phase can be ignored, and no inrush currents occur in the fault response. However, 2) with DSC, the response speed is much slower (i.e., about 60ms), and there exist inrush currents with a value of about 2.2 p.u. to be harmful to the protection systems and other equipment installed in the grid. Thus, it is very meaningful to analyze the fault response of IIGs with DSC in detail to obtain the peak value, peak time, and the transient period of the inrush current for the power system design and the protection system setup. The peak value is the maximum value of the inrush current,

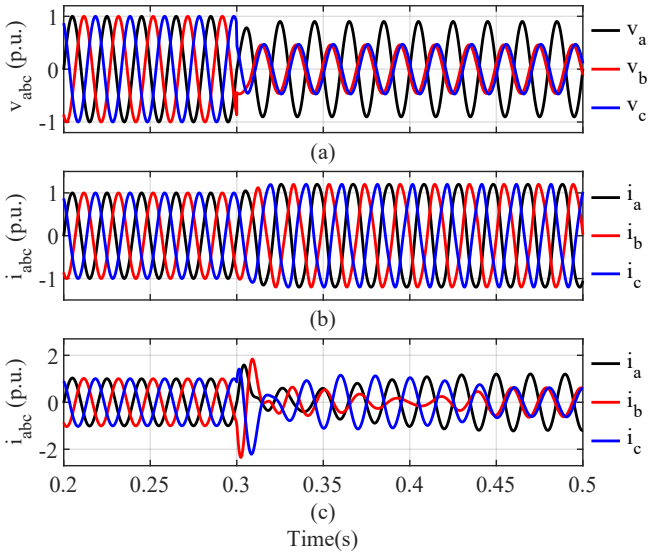

Fig. 8. Fault responses comparison of IIGs with DSC and DCC. (a) The grid voltage of the connected bus of IIGs. (b) The fault current of the IIG with DCC. (c) The fault current of the IIG with DSC.

and the peak time is the period from fault beginning to the time when the fault current reaches its maximum value.

2) Verification under various fault conditions: Three sub-cases are established to verify the correctness and the applicability of the proposed model. The results are shown in Fig. 9 - 11.

Fig. 9 shows the simulation and calculated results of fault responses of IIGs with DSC under various types of faults including the single-phase to ground fault, the two-phase to ground fault, the three-phase to ground fault, and the two phase short-circuit fault. In Fig. 9, the faults occur at 0.3; the solid and dash lines in every sub-figure represent the simulated and calculated fault currents, respectively. From Fig. 9, it can be observed that 1) the simulated and calculated fault currents under various types of faults almost coincide; 2) the amplitude of fault currents keeps increasing in approximately a quarter of one cycle (5 ms), and then reduces to the limited value; 3) the peak value and the peak time of the inrush current are affected by the fault types.

Fig. 10 and Fig. 11 present simulation and calculation results under different voltage digs and bandwidth of controllers to verify the proposed model. In both case studies, the most terrible fault, three-phase to ground fault is applied to the simulation. In the case whose results are shown in Fig. 10, the bandwidth of the current controller is 80 Hz, and in the case

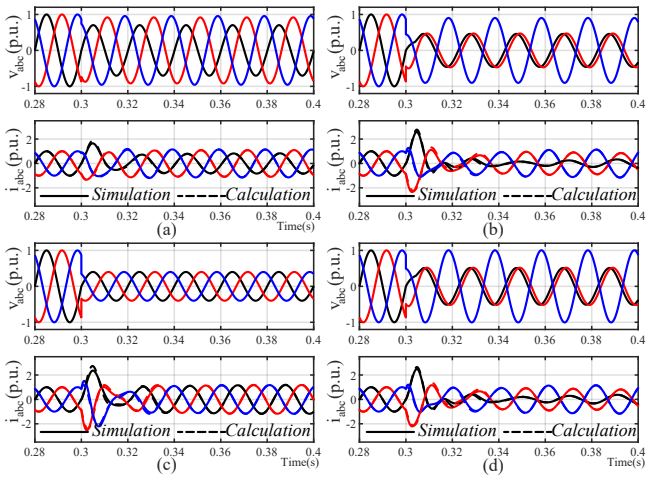

Fig. 9. The verification of the proposed model with different type of faults. (a) Single-phase (A) to ground faults. (b) Two-phases (AB) to ground faults. (c) Three-phases to ground faults. (d) Two-phases (AB) short-circuit faults.

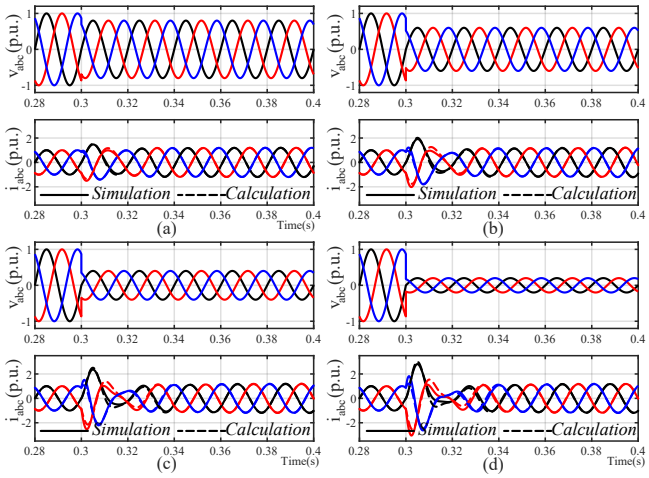

Fig. 10. The verification of the proposed model with different voltage dips. (a) Voltage dips to 80%. (b) Voltage dips to 60%. (c) Voltage dips to 40%. (d) Voltage dips to 20%.

whose results are shown in Fig. 11, the voltage dips to 0.5 p.u.. It can be seen in Fig. 10 - 11, the inrush current increases with the increase of voltage dips, and it reduces with the increase of bandwidth of the current controller. The calculation result is almost coincident with the simulation result in both figures, which means the proposed model is correct to analyze the fault response of IIGs with DSC with different voltage dips and bandwidth of the current controller.

The proposed model introduces simplification to reduce the complexity, meanwhile, inevitable errors are also introduced to the calculation result. Table III - V present the error of results shown in Fig. 9 – 11. It can be seen in these tables, the maximum error of all case studies is less than 10%, which is a normally acceptable region of errors in the fault analysis of the power system. The error analysis shows that the proposed model is correct enough to analyze the fault response of IIGs with DSC.

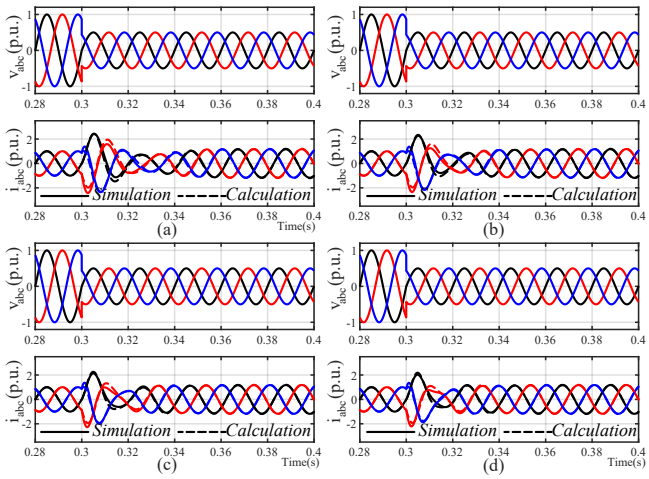

Fig. 11. The verification of the proposed model with different bandwidth of current controllers. (a) The bandwidth is 40 Hz. (b) The bandwidth is 60 Hz. (c) The bandwidth is 80 Hz. (d) The bandwidth is 100 Hz.

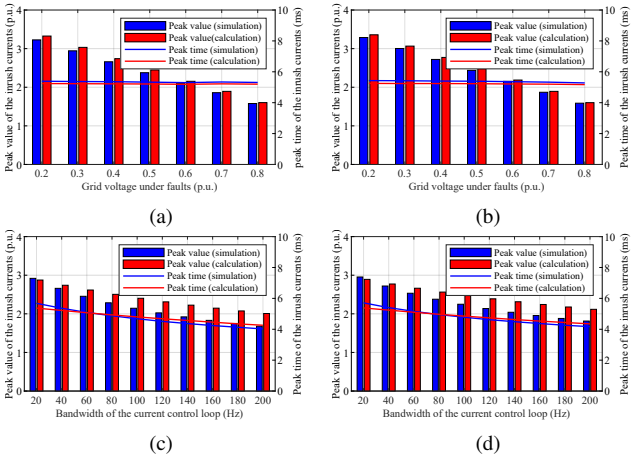

Fig. 12. The influence of voltage sag, controller parameters and LVRT strategies on fault responses of IIGs. (a) The influence of voltage sag on fault responses of IIGs under enabled LVRT controller. (b) The influence of voltage sag on fault responses of IIGs under disabled LVRT controller. (c) The influence of the bandwidth of controller on fault responses of IIGs under enabled LVRT controller. (d) The influence of the bandwidth of controller on fault responses of IIGs under disabled LVRT controller.

TABLE III
ERROR ANALYSIS OF THE RESULT SHOWN IN FIG. 9.

Fault Type	Peak value error (%)	Peak time error (%)
Single-phase to Ground	2.73	0.26
Two-phase to Ground	6.12	0.4
Three-phase to Ground	7.36	0.86
Two-phase Short-circuit	6.27	0.42

TABLE IV
ERROR ANALYSIS OF THE RESULT SHOWN IN FIG. 10.

Sub-cases	Peak value error (%)	Peak time error (%)
Sub-case (a)	3.46	0.78
Sub-case (b)	5.10	0.60
Sub-case (c)	6.12	0.40
Sub-case (d)	6.82	0.20

TABLE V
ERROR ANALYSIS OF THE RESULT SHOWN IN FIG. 11.

Sub-cases	Peak value error (%)	Peak time error (%)
Sub-case (a)	0.29	3.5
Sub-case (b)	3.24	1.73
Sub-case (c)	5.67	0.40
Sub-case (d)	7.67	0.41

3) Other influences on the fault response: Fig. 12 shows the simulated and calculated results to illustrate the influence of voltage sags, bandwidth of the current controller and LVRT controller on the fault response of IIGs with DSC under the three-phase-to-ground fault. In Fig. 12, the bar-plot is used to show the peak value and the peak time of the inrush current.

From Fig. 12(a), it can be seen that the peak value of the inrush current increases almost linearly with the extent of the voltage sag, and the peak time of the inrush current keeps constant. Thus, it can be concluded that the voltage sag has an influence on the peak value and has no influence on the peak time of the inrush current. From Fig. 12(c), it can be seen that the peak value of the inrush current is affected by the bandwidth of the current controller (i.e., the larger the bandwidth, the smaller the peak value of the inrush current becomes). In addition, the peak time of the inrush current is slightly affected by the bandwidth of current controller, and it reduces with the bandwidth increase.

Fig. 12(b) and Fig. 12(d) illustrate the influence of LVRT controller on the transient of fault responses. In Fig. 12(b) and Fig. 12(d), the reference input of the current controller is generated by the power controller and the current limiter because the LVRT is disabled. Comparing Fig. 12(a) with Fig. 12(b), it can be observed that the LVRT controller has a very slight influence on the peak value and the peak time of the inrush current. This can be also obtained through comparing Fig. 12(c) with Fig. 12(d).

It can be observed from Fig. 12(c) and 12(d) that the peak time and value estimation are diverging with an increase in the bandwidth of the current controller. This phenomenon comes because of the simplification used in the proposed model. The simplification of the coupled system used in the proposed approach is based on the time constant of the sub-system, and the error caused by the simplification is strongly related to the input. In the closed-loop control, the error is fed back to the controller and thus, if a greater bandwidth of the controller is used, the output of the controller becomes greater, which results in the error of the proposed model increases with the increase of the bandwidth. However, based on the PI parameters design rule discussed in the above section, the bandwidth of the current controller of IIGs with DSC is normally less than 100 Hz. As the result shown in Fig. 11 and the error shown in Tab. V, when the bandwidth is set to 100 Hz, the error of the proposed model is 7.67%, which is acceptable in the fault analysis. Therefore, the error caused by the bandwidth is acceptable to analyze the fault response of IIGs with DSC in practical applications.

TABLE VI
PARAMETERS OF EXPERIMENTAL PLATFORM.

Parameters	Values
Rated grid voltage	380 V
Rated power	10 kVA
Voltage of DC source	750 V
System frequency	50 Hz
Total resistance of the power filter	62 mΩ
Total inductance of the power filter	4.2 mH
Cutoff frequency of current controller	80 Hz
Switching frequency	10 kHz
Sampling frequency	10 kHz
dSPACE processor board	DS1006
dSPACE digital IO board	DS5101

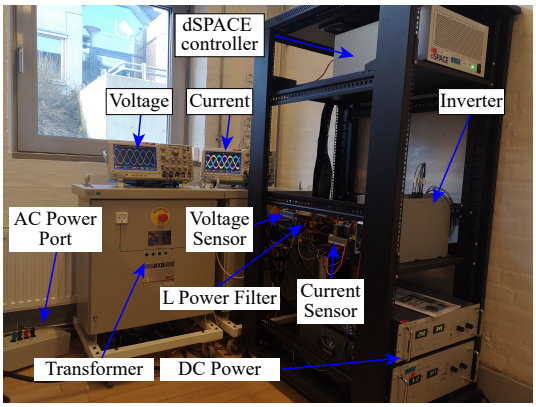

Fig. 13. The experimental platform.

B. Experimental Verification

To verify the proposed model, a 10 kVA IIG experiment platform as shown in Fig. 13 is established. The hardware topology and parameters of the experiment platform are shown in Fig. 1 and Table VI. The power filter is L filter. It is a 10 kVA-DYn11 transformer with 1:1 transfer ratio used in the platform. The fault is assumed located at bus B_1, which voltages are generated by the three-phase power source *California Instruments MX-35*. The controller is established by using the dSPACE.

Fig. 14 presents the comparison between the experimental and calculation results under different types of faults. The bandwidth of the controller is 80 Hz. From Fig. 14, it can be observed that the calculation waveform is coincident with the experimental result under grid fault conditions.

Fig. 15 - 16 present the comparison between experimental results and calculation results under different voltage dips and bandwidth of controllers. The most terrible fault, three-phase to ground fault is applied in the case studies. The voltage dips and band-width of current controllers are added to the figure as legends. It can be seen that in Fig. 15 - 16, the calculated results are almost coincident with the experimental results, which means the proposed model has good performance in the fault analysis of IIGs with DSC.

It can be seen in Fig. 14 - 16 that there exist small errors in results. These small errors come from the proposed model itself and on the other hand, from some uncontrollable factors

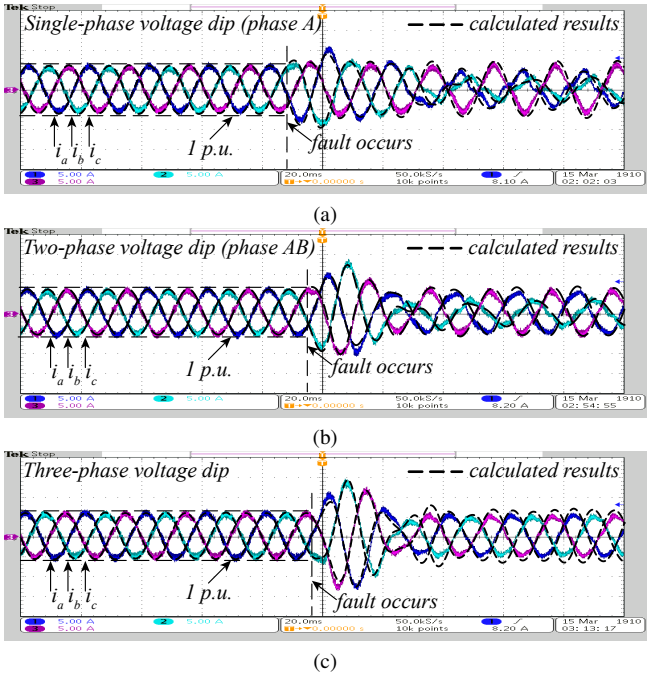

Fig. 14. The comparisons between experimental and calculation currents under different type of faults: (a) Single-phase voltage dip; (b) Two-phase voltage dip; (c) Three-phase voltage dip.

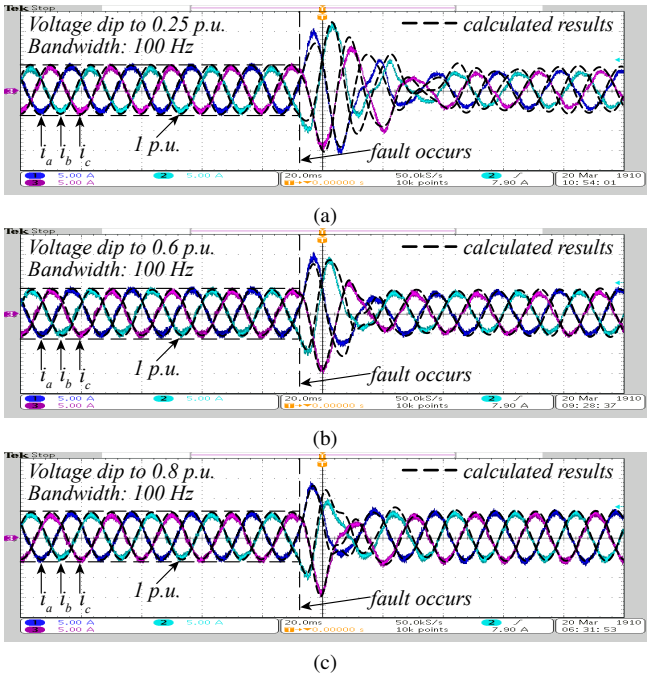

Fig. 15. The comparisons between experimental and calculation currents under different voltage dips when the bandwidth of the current controller is 200 Hz: (a) Voltage dips to 0.25; (b) Voltage dips to 0.6; (c) Voltage dips to 0.8.

in the practical experiment, e.g., sampling errors, calculation errors caused by dSPACE, and the fault time error. Thus, the error of the proposed model is smaller than the error shown in Fig. 14 - 16 in practice.

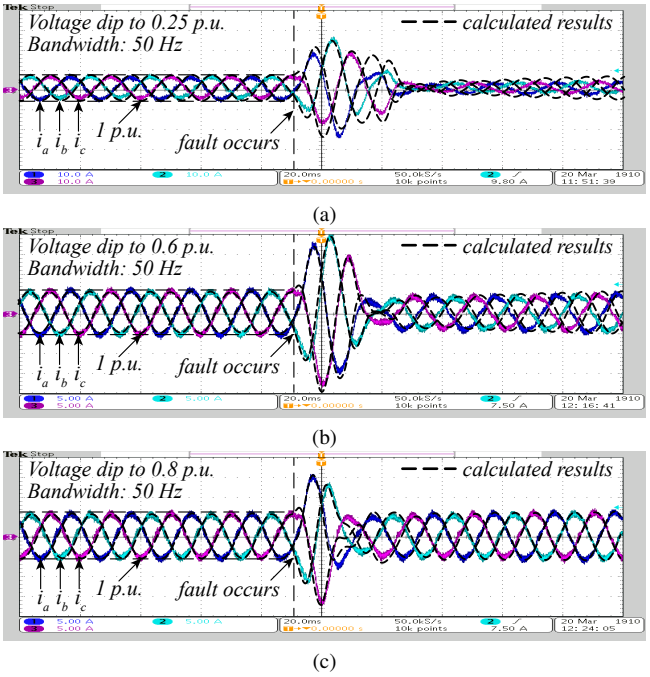

Fig. 16. The comparisons between experimental and calculation currents under different voltage dips when the bandwidth of the current controller is 100 Hz: (a) Voltage dips to 0.25; (b) Voltage dips to 0.6; (c) Voltage dips to 0.8.

V. Conclusion

This paper proposes an analytic model for the fault analysis of IIGs with DSC. Based on the proposed model, the fault characteristics of the IIG with DSC are analyzed in detail with the consideration of LVRT. The proposed model is validated by simulation and experimental results. Main observations and contributions of this study are briefly concluded as follows.

(1) The proposed analytic model can effectively calculate fault responses of IIGs with DSC, which is usually obtained by EMT simulation. Also, the proposed model can analyze impacts from controller parameters, delays of the control system, and LVRT strategy on fault responses. More importantly, the proposed model provides a basis for the LVRT control strategy, the power filter design, and the protection system setup.

(2) The inrush current appearing in the fault response of IIGs is mainly caused by the delay of the control system. If the delay of the control system is fixed, there are three factors affecting the inrush current: the bandwidth of current controllers, the degree of voltage sag, and the inductance of the power filter.

(3) The peak time of inrush currents is mainly affected by the bandwidth of current controllers. The correlation between them is negative. The peak value of inrush currents can be affected by the above three factors. The peak value has a negative relationship with the bandwidth of current controllers and the inductance of the power filter, but has a positive relationship with the degree of voltage sag.

(4) The LVRT control strategy has a slight influence on the transient of fault responses. The peak value and the peak time of inrush currents keep almost constant when the

LVRT is enabled or disabled. However, it would affect the steady-state fault currents.

REFERENCES

[1] I. T. F. on Short-Circuit and S. P. I. of Inverter Based Generation, "Impact of inverter based generation on bulk power system dynamics and short-circuit performance," IEEE Power and Energy Society, New Jersey, USA, Tech. Rep. PES-TR68, Sep. 2018.

[2] M. Behnke and A. Ellis, "Contribution of photovoltaic power generation systems to ac short circuits — a survey of current modeling practices and challenges," in *Proc. IEEE 39th Photovoltaic Specialists Conference (PVSC)*, DOI 10.1109/PVSC.2013.6745121, pp. 3128–3133, Florida, USA, Jun. 2013.

[3] Z. Liang, X. Lin, Y. Kang, B. Gao, and H. Lei, "Short circuit current characteristics analysis and improved current limiting strategy for three-phase three-leg inverter under asymmetric short circuit fault," *IEEE Trans. Power Electron.*, vol. 33, DOI 10.1109/TPEL.2017.2759161, no. 8, pp. 7214–7228, Oct. 2018.

[4] N. Nimpitiwan, G. T. Heydt, R. Ayyanar, and S. Suryanarayanan, "Fault current contribution from synchronous machine and inverter based distributed generators," *IEEE Trans. Power Del.*, vol. 22, DOI 10.1109/TPWRD.2006.881440, no. 1, pp. 634–641, Dec. 2007.

[5] M. E. Baran and I. M. El-Markaby, "Fault Analysis on Distribution Feeders With Distributed Generators," *IEEE Trans. Power Syst.*, vol. 20, DOI 10.1109/TPWRS.2005.857940, no. 4, pp. 1757–1764, Oct. 2005.

[6] L. He, Z. Shuai, X. Zhang, X. Liu, Z. Li, and Z. J. Shen, "Transient characteristics of synchronverters subjected to asymmetric faults," *IEEE Trans. Power Del.*, vol. 34, DOI 10.1109/TPWRD.2019.2906766, no. 3, pp. 1171–1183, Mar. 2019.

[7] M. Brucoli, T. C. Green, and J. D. F. McDonald, "Modelling and analysis of fault behaviour of inverter microgrids to aid future fault detection," in *Proc. IEEE International Conference on System of Systems Engineering*, DOI 10.1109/SYSOSE.2007.4304253, pp. 1–6, Texas, USA, Sep. 2007.

[8] W. Guo, L. Mu, and X. Zhang, "Fault Models of Inverter-Interfaced Distributed Generators Within a Low-Voltage Microgrid," *IEEE Trans. Power Del.*, vol. 32, DOI 10.1109/TPWRD.2016.2541344, no. 1, pp. 453–461, Mar. 2017.

[9] Z. Shuai, C. Shen, X. Yin, X. Liu, and Z. J. Shen, "Fault Analysis of Inverter-Interfaced Distributed Generators With Different Control Schemes," *IEEE Trans. Power Del.*, vol. 33, DOI 10.1109/TPWRD.2017.2717388, no. 3, pp. 1223–1235, Jun. 2018.

[10] J. Jia, G. Yang, and A. H. Nielsen, "A review on grid-connected converter control for short-circuit power provision under grid unbalanced faults," *IEEE Trans. Power Del.*, vol. 33, DOI 10.1109/TPWRD.2017.2682164, no. 2, pp. 649–661, Mar. 2018.

[11] B. Mahamedi and J. E. Fletcher, "The Equivalent Models of Grid-Forming Inverters in the Sequence Domain for the Steady-State Analysis of Power Systems," *IEEE Trans. Power Syst.*, vol. 35, DOI 10.1109/TPWRS.2020.2968114, no. 4, pp. 2876 – 2887, Jul. 2020.

[12] T. Kauffmann, U. Karaagac, I. Kocar, S. Jensen, E. Farantatos, A. Haddadi, and J. Mahseredjian, "Short-Circuit Model for Type-IV Wind Turbine Generators With Decoupled Sequence Control," *IEEE Trans. Power Del.*, vol. 34, DOI 10.1109/TPWRD.2019.2908686, no. 5, pp. 1998–2007, Apr. 2019.

[13] Q. Zhong, Q. Shi, G. Wang, and H. Li, "Short circuit analysis of PV inverter under unbalanced conditions with dynamic phasor sequence components," in *2016 IEEE PES General Meeting*, DOI 10.1109/PESGM.2016.7741115, pp. 1–5, MA, USA, Jul. 2016.

[14] X. Kong, Z. Zhang, and X. Yin, "Fault Current Study of Inverter Interfaced Distributed Generators," *Distributed Generation & Alternative Energy Journal*, vol. 30, DOI 10.1080/21563306.2015.11461420, no. 3, pp. 6–26, Jul. 2015.

[17] C. A. Plet, "Fault Response of Inverter-Based Distributed Generation," PhD, Department of Electrical and Electronic Engineering, London, UK, 2011.

[15] C. A. Plet and T. C. Green, "Fault response of inverter interfaced distributed generators in grid-connected applications," *Electric Power Systems Research*, vol. 106, DOI 10.1016/j.epsr.2013.07.013, pp. 21–28, Sep. 2014.

[16] C. A. Plet, M. Graovac, T. C. Green, and R. Iravani, "Fault response of grid-connected inverter dominated networks," in *2010 IEEE PES General Meeting*, DOI 10.1109/PES.2010.5589981, pp. 1–8, RI, USA, Jul. 2010.

[18] C. A. Plet, M. Brucoli, J. D. F. McDonald, and T. C. Green, "Fault models of inverter-interfaced distributed generators: Experimental verification and application to fault analysis," in *2011 IEEE PES General Meeting*, DOI 10.1109/PES.2011.6039183, pp. 1–8, MI, USA, Jul. 2011.

[19] G. Kou, Le Chen, P. VanSant, F. Velez-Cedeno, and Y. Liu, "Fault Characteristics of Distributed Solar Generation," *IEEE Trans. Power Del.*, vol. 35, DOI 10.1109/TPWRD.2019.2907462, no. 2, pp. 1062 – 1064, Mar. 2020.

[20] R. Teodorescu, M. Liserre, and P. Rodriguez, *Grid converters for photovoltaic and wind power systems*, vol. 29. John Wiley & Sons, 2011.

[21] L. Harnefors, M. Bongiorno, and S. Lundberg, "Input-admittance calculation and shaping for controlled voltage-source converters," *IEEE Trans. Ind. Electron.*, vol. 54, DOI 10.1109/TIE.2007.904022, no. 6, pp. 3323–3334, Nov. 2007.

[22] U. Karaagac, J. Mahseredjian, H. S. H. Gras, J. Peralta, and L. D. Bellomo, "Simulation models for wind parks with variable speed wind turbines in emtp-rv," Polytechnique Montréal, Montreal, QC, Canada, Tech. Rep. User's Manual, EMTP-RV Software ver. 4.0.2, Apr. 2019.

[23] T. Furuhashi, S. Okuma, and Y. Uchikawa, "A study on the theory of instantaneous reactive power," *IEEE Trans. Ind. Electron.*, vol. 37, no. 1, pp. 86–90, Feb. 1990.

[24] Hong-Seok Song and Kwanghee Nam, "Dual current control scheme for pwm converter under unbalanced input voltage conditions," *IEEE Trans. Ind. Electron.*, vol. 46, no. 5, pp. 953–959, Oct. 1999.

[25] R. Kabiri, D. G. Holmes, and B. P. McGrath, "Control of active and reactive power ripple to mitigate unbalanced grid voltages," *IEEE Trans. Ind. Appl.*, vol. 52, DOI 10.1109/TIA.2015.2508425, no. 2, pp. 1660–1668, Dec. 2016.

[26] Energinet. DK, "Technical regulation 3.2.5 for wind power plants above 11 kw," Energinet. DK, Denmark, Tech. Rep. 13/96336-43, Jul. 2016.

[27] M. Nagpal and C. Henville, "Impact of power-electronic sources on transmission line ground fault protection," *IEEE Trans. Power Del.*, vol. 33, DOI 10.1109/TPWRD.2017.2709279, no. 1, pp. 62–70, May. 2018.

[28] I. Erlich, T. Neumann, F. Shewarega, P. Schegner, and J. Meyer, "Wind turbine negative sequence current control and its effect on power system protection," in *2013 IEEE Power Energy Society General Meeting*, DOI 10.1109/PESMG.2013.6672880, pp. 1–5, BC, Canada, Jul. 2013.

[29] P. Rodríguez, A. Luna, I. Candela, R. Mujal, R. Teodorescu, and F. Blaabjerg, "Multiresonant frequency-locked loop for grid synchronization of power converters under distorted grid conditions," *IEEE Trans. Ind. Electron.*, vol. 58, DOI 10.1109/TIE.2010.2042420, no. 1, pp. 127–138, Apr. 2011.

[30] J. R. Carson, "Notes on the theory of modulation," *Proceedings of the Institute of Radio Engineers*, vol. 10, DOI 10.1109/JRPROC.1922.219793, no. 1, pp. 57–64, Feb. 1922.

[31] A. Varga, "Balancing free square-root algorithm for computing singular perturbation approximations," in *1991 Proceedings of the 30th IEEE Conference on Decision and Control*, DOI 10.1109/CDC.1991.261486, pp. 1062–1065 vol.2, Brighton, UK, Dec. 1991.